Supporting Information

Effect of Surface Hydrogenation of Metal Oxides on the Nanomorphology and the Charge Generation Efficiency of Polymer Blend Solar Cells

Maria Vasilopoulou

Institute of Nanoscience and Nanotechnology (INN), National Centre for Scientific Research "Demokritos", 153 10, Aghia Paraskevi Attikis, Athens, Greece.

Email: mariva@imel.demokritos.gr

Table of Contents

S1. Comparative study on WO_x and OH-WO_x films: Structure ans Electric Transport

S1.1 X-ray (XPS) and ultraviolet (UPS) photoelectron spectra

Under-stoichiometric tungsten oxides were deposited using a hot-wire deposition method in reducing ambient (N_2 environment with hydrogen pulses). Then, films were annealed at 450 ^oC for about 5 hours in hydrogen poor environment, in particular forming gas (FG, 90 % N_2 and 10% H_2) or hydrogen rich environment (pure hydrogen). XPS analysis was performed in order to investigate the chemical composition of the outermost film layers. The W 4f photosignals of the XPS spectra of the tungsten oxide samples grown in FG (termed hereafter as WO_x) and H_2 (termed hereafter as OH-WO_x), are presented in Figure S1 a and c, respectively.

For the film annealed in FG (Fig. S1 a) the deconvolution of the W 4f photoemission peak was performed using two distinct doublets; the first doublet exhibits two peaks with nearly equal width (FWHM=1.7 eV) with the binding energy (BE) of W $4f_{7/2}$ centered at 36.0±0.1 eV and that of W $4f_{5/2}$ appear at BE 38.2±0.1 eV (with a peak ratio of 4:3). The position and the shape of these peaks are representative of W atoms with an oxidation state +6.[1] Apart from the major components arising from W^{6+}, a second doublet at lower BEs (BE of (W $4f_{7/2}$) =34.8 eV, and of (W $4f_{5/2}$) =37.1 eV with FWHM=1.8 eV and a peak ratio 4:3), corresponding to 25% of the overall W, was detected. This new doublet is attributed to the presence of W^{+5} atoms, indicating that these films are under-stoichiometric.[2] The film annealed in H_2 exhibits quite similar XPS W 4f core levels spectrum with than annealed in FG (Fig. S1 c). It was also found under-stoichiometric with the contribution of peaks attributed to W^{5+} states in their XPS W 4f spectrum to be ~ 27% of the total, respectively. A summary of the different metal oxides of this study is shown in Table S1, along with the percentage of various oxidation states of the metal cation.

A similar work was done to O1s peaks to discriminate different oxygen species (Figure S1 b, d). In the deconvoluted XPS O1s spectra of the sample annealed in FG, we observed the lattice oxygen peak (O^{2-}) located at about 530.6 eV and a broader water (H_2O) shoulder at around 532.4 eV.[3] In the O 1s XPS spectrum of the film annealed in H_2, although it still exhibits the O^{2-} and H_2O peaks, a significant contribution from a third peak at around 531.5 eV is observed which can be assigned to hydroxyl (OH^-) groups bonded with metal cations present on the metal oxide surface.[3] According to these results it becomes

obvious that films annealed in H_2 exhibit a higher amount of surface hydrogen content than those annealed in FG, in the form of hydroxyl groups either in adsorbed water molecules or bonded to surface metal cations.

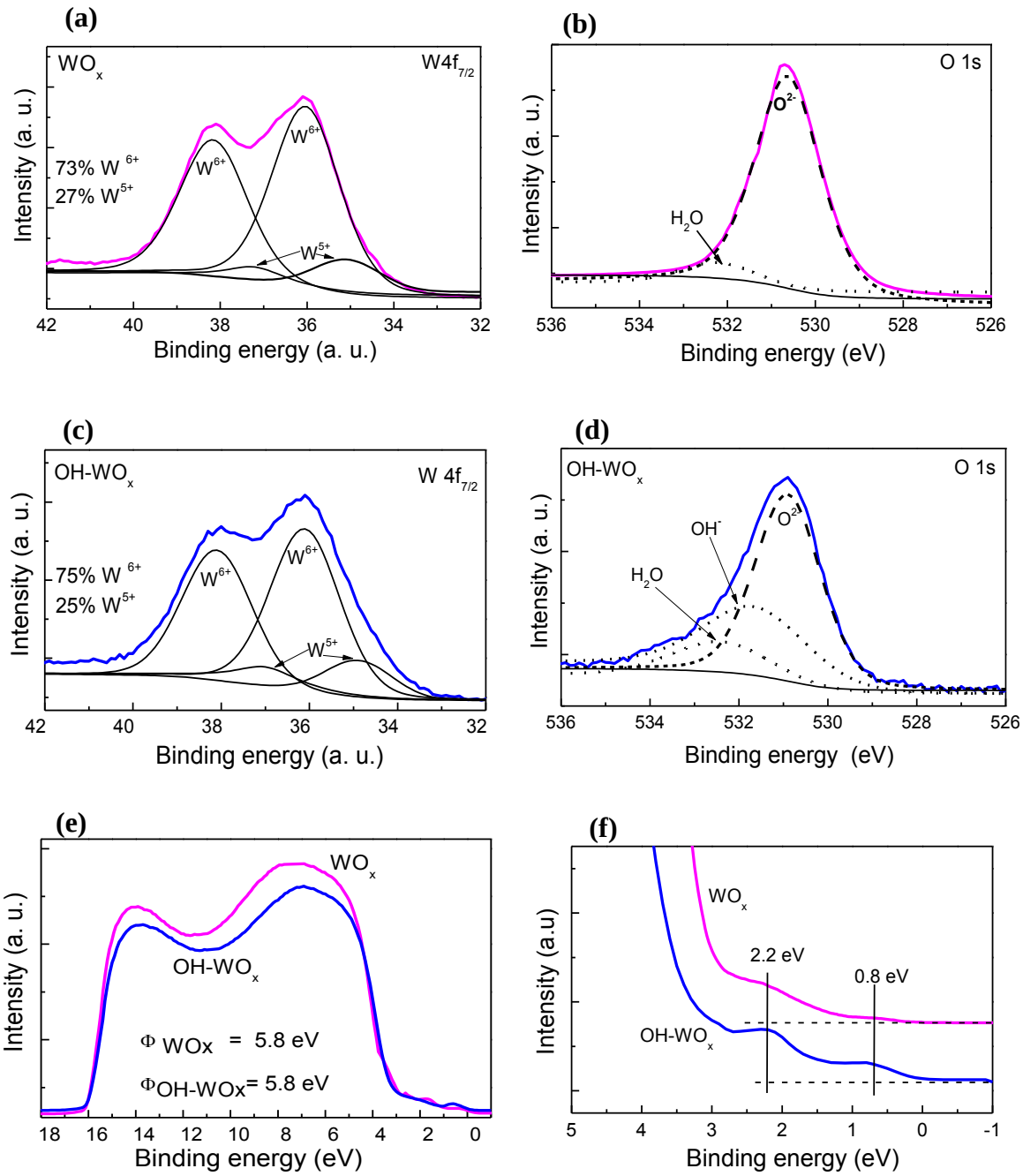

Figure S1 XPS (and fittings) and UPS spectra of tungsten oxides annealed in environment containing low (WO_x) and high hydrogen content (OH-WO_x). (a) and (c) W 4f XPS core levels and (b) and (d) O 1s core leves of WO_x and OH-WO_x, respectively. (e) The valence band spectra derived from UPS measurements taken on WO_x and OH-WO_x films. (f) The near Fermi level region of the UPS spectra.

Figure S1 e, f shows the UPS spectra and the low binding energy region of these spectra, respectively, of the outermost layer of the aforementioned tungsten oxide films. The valence band maximum (VBM) in both

films is located at 3.0± 0.1 eV below the Fermi level and since the band gap is 3.45 eV (derived from optical absorption measurements, not shown), the materials are negatively (n) doped. This is due to the under-stoichiometry of the samples imposed by thermodynamics and in view of the huge difference between the atomic weights of tungsten and oxygen. It can be observed that the states related to oxygen defects appear just above the edge of the VB and spread in the band gap decreasing with energy in agreement with previous works.[4] The spectrum of film annealed in FG exhibits a significant density of occupied gap states exhibiting two local maxima at approximately 2.2 and 0.8 eV below the Fermi level. These states can be attributed to oxygen vacancies or/and hydrogen dopants. In the UPS spectrum of the film annealed in H_2 the density of states becomes higher probably due to the larger amount of hydrogen atoms present in the material surface and/or outermost layer. Finally, from the secondary electron cut-off of the UPS spectra a work function (W_F) value equal to 5.8 eV for each film can be estimated.

S1.2 Raman and FTIR measurements

The evolution of room temperature Raman spectra for the tungsten oxide samples annealed in different environments, are shown in Figure S2 a. It is observed that the 816 cm^{-1} mode increases significantly relative to the 710 cm^{-1} mode upon annealing in H_2 environment, as a result of surface hydrogenation. Another interesting aspect of the Raman spectra is a dependence of the stretching mode frequency on surface hydrogen content: upon increased surface hydrogenation (annealing in H_2), the stretching frequencies increase (e. g., to 816 cm^{-1} from 806 cm^{-1} for the n(W–O) stretching) when compared with the sample annealed in FG (low hydrogen environment). It is known that the force constant (and thus the stretching frequencies and the length of the bonds are strongly correlated. In the tungsten oxide with the high surface hydrogen content a distortion of the surface lattice due to hydrogen bonding may result in the observed shift of the stretching mode frequencies.

In Figure S2 b FTIR spectra taken on the tungsten oxide samples annealed in FG and H_2 environments, are shown. Typically, the FTIR spectra of tungsten oxide layers within the range 400-4000 cm^{-1} may be roughly divided in four regions:[6] 400-500 cm^{-1} where the vibration modes of the W-O bond are manifested, 500-1100 cm^{-1} related to the vibration of the W-O-W and O-W-O chains, 1300-1800 cm^{-1} related to the

vibrations of H-O-H and W-OH and 3000-3600 cm^{-1} where vibrations due to the presence of W-OH and of adsorbed H_2O appear. The spectrum of the sample annealed in FG exhibits the above typical features with an additional shoulder near 910 cm^{-1} attributed to the W=O bond and small peaks observed at the region near 1590 cm^{-1}, which as mentioned above, are related to vibrations of H-O-H chains and of W-OH. These peaks are even more pronounced in the spectrum of the film annealed in H_2 environment. The existence of O-H bonds either in form of water or of hydroxyl radicals is in agreement with the conclusions drawn from the XPS measurements presented above. The presence of water in sample is also evidenced by the multiple peaks observed within the range 3200-3900 cm^{-1}. These multiple peaks were attributed in the past to the formation of hydrogen bonds between the OH groups in films.

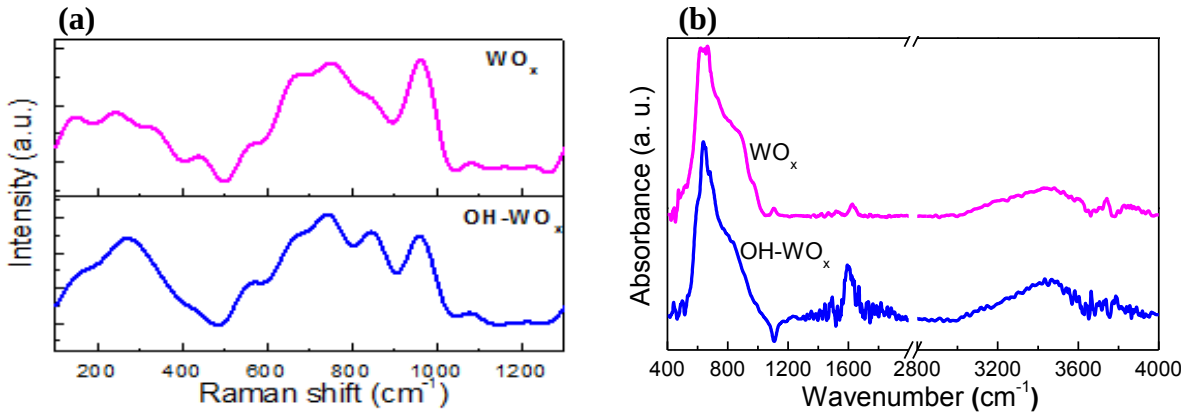

Figure S2. (a) Raman and (b) FTIR spectra taken on tungsten oxide samples deposited in environment containing low (WO_x) and high hydrogen content (OH-WO_x).

S1.3 Photoluminescence spectra and conductivity measurements

In Figure S3 a the PL spectra for the tungsten oxide films annealed in FG and H_2 environments, are shown. The exact composition and the microstructure of samples are expected to influence the exact positioning of the PL peaks due to quantum confinement effects.[7] It is seen that, the samples exhibit different PL emission with the PL spectrum of the second film to show similarities with others found in literature related to tungsten oxide samples grown form aquatic solutions, which most probably also contain such species and to the spectrum of a sample composed by $WO_3.H_2O$.

The transport properties of the two tungsten oxide films were also investigated through measuring the electrical resistivity at various temperatures (above room temperature). From Figure S3 b it is obvious that both films show quite similar dependence of their resistivity with temperature with the one annealed in H_2 to exhibit slightly smaller resistivity compared with its FG annealed counterpart.

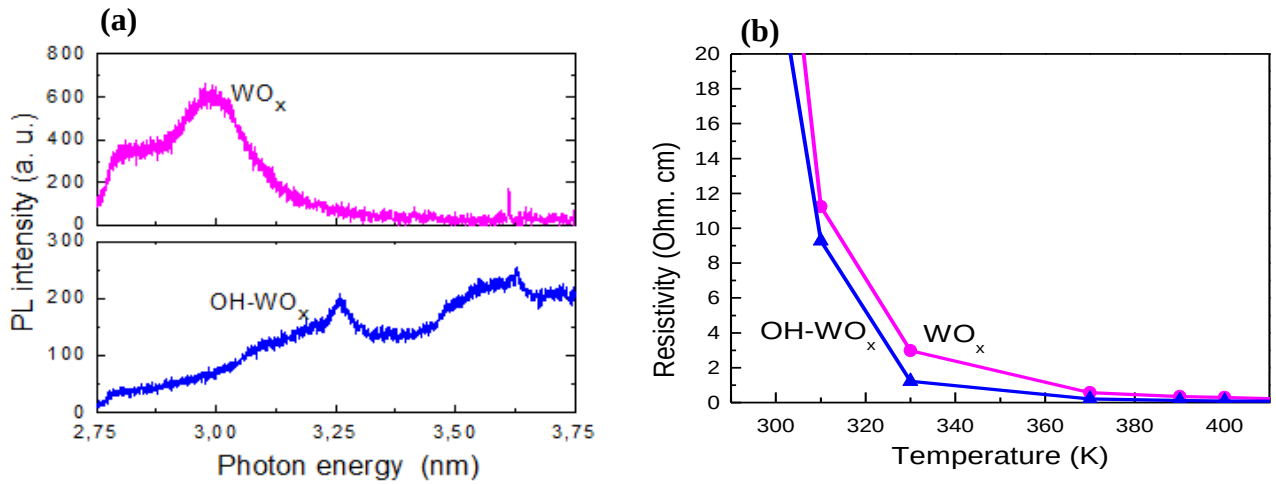

Figure S3. (a) Photoluminescence spectra taken on tungsten oxides deposited under the same conditions and annealed in environment containing low (WO_x) and high hydrogen content (OH-WO_x) with excitation radiation of 3.81 eV. (b) Resistivity measurements vs temperature for both tungsten oxide, 10 nm thin films.

S2. Comparative study on MoOx and OH-MoOx films: Structure ans Electric Transport

S2.1 X-ray (XPS) and ultraviolet (UPS) photoelectron spectra

As in the case of tungsten oxides, molybdenum oxide films were deposited in reducing ambient using the hot-wire method and then annealed at 450 ^oC for 5 h in either FG or H_2 environment. The chemical composition of each film was determined by analyzing the XPS spectra of the Mo 3d core level peaks shown in Figure S4 a and c, respectively. Oxide identification is accomplished from the shift of the Mo 3d core levels with regard to its stoichiometric form and by calculating the ratio between the Mo^{6+} component versus the Mo components with lower oxidation states (5+, 4+). From these data it can be deduced that both films are under-stoichiometric with the degree of oxide reduction to be slightly lower for the one annealed in FG. Indeed, the Mo 3d core level spectrum of the MoO_x (Fig. S4 a) consists except of the spin-orbit doublet with peaks at 232.4 eV and 235.7 eV BE, associated with Mo cations in the higher oxidation state (Mo^{6+}),[8] also

of a second doublet (Mo $3d_{5/2}$ at 231.6 eV and Mo $3d_{3/2}$ at 234.9 eV BE) which indicates the presence of the Mo^{5+} lower oxidation state accounting for 22% of the total Mo states. The Mo 3d core level spectrum of the hydrogen annealed (OH-MoO_x, Fig. S4 c) is quite similar to that of MoO_x but it exhibits a slightly decreased ratio of Mo^{5+} oxidation states, now accounting for 24% of the total Mo states (Table S1).

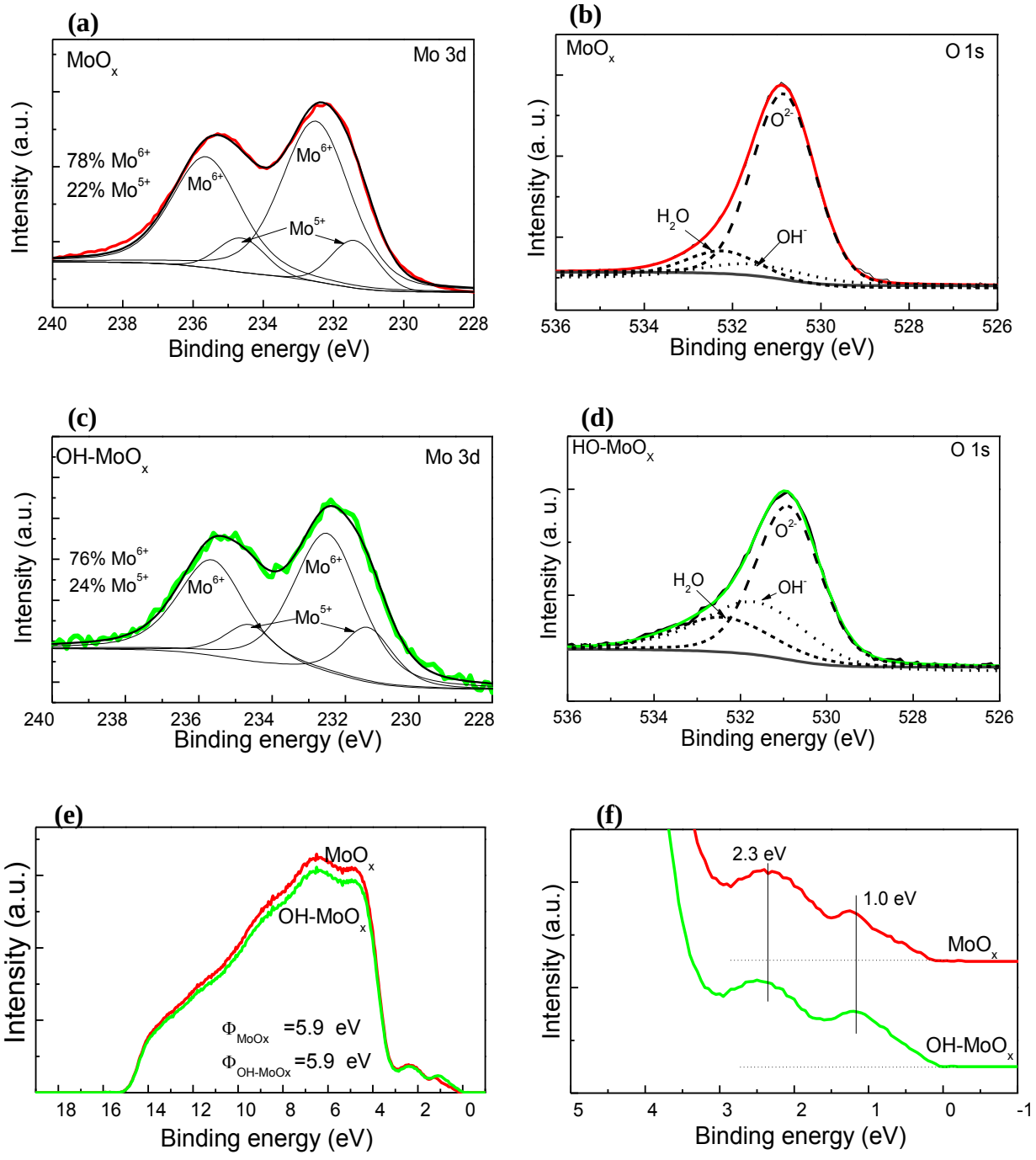

Figure S4 XPS (and fittings) and UPS spectra of molybdenum oxides deposited in environment containing low (MoO_x) and high hydrogen content (OH-MoO_x). (a) and (c) Mo 3d XPS core levels and (b) and (d) O 1s core leves of MoO_x and OH-MoO_x, respectively. (e) The valence band spectra derived from UPS measurements taken on MoO_x and OH-MoO_x films. (f) The near Fermi level region of the UPS spectra.

The O 1s photoemission peaks (Figure S4 b and d) of the above oxides are consisting of a main peak at 530.4 eV and is assigned to the typical Mo-O bond. However, the deconvolution process in the O 1s region of the hydrogen Mo oxides reveal an extra peak (beyond the typical oxide region) at 531.5 eV, which could be assigned to hydroxyl groups (-OH) incorporated within the oxides in the form of Mo-OH surface species and a broader water (H_2O) shoulder at around 532.4 eV. In the O 1s XPS spectrum of the film annealed in H_2, the contribution of the peak attributed to OH- groups bonded to surface metal cations is highly significant (Table S1).

Further studies on the electronic structure of Mo oxides annealed in different deposition environments were performed by UPS. The valence band spectra are shown in Figure S4 e, whereas the expanded view of the valence band is shown separately in Figure S4 e. Both Mo oxide films exhibit very similar UPS spectra with a W_F equal to 5.9 eV (as derived from the secondary electron cut-off), the valence band onset at about 3.0 eV and the appearance of broad features near the E_F, which are centred at 2.2 eV and at 1.1 eV. These bands are indicative of new occupied states forming inside the band gap with a relatively large density. Note that both Mo oxides exhibit an optical bandgap equal to 3.1 eV as derived from optical absorption measurements (not shown).

S2.2 Raman and FTIR measurements

To further identify Mo oxides structure Raman spectroscopy was performed on several materials formulated in different environments (Figure S5 a). In general, for a stoichiometric Mo oxide film three main characteristic bands at 956 cm^{-1} assigned to the stretching vibration of terminal oxygens (νO═Mo), at 875 cm^{-1} assigned to the stretching mode of doubly coordinated oxygens (νO−Mo_2), and at 751 cm^{-1} attributed to the stretching mode of triply coordinated oxygens (νO−Mo_3), are expected.[9,10] In our Mo oxides, all these bands appear shifted to lower wavenumbers, especially for the Mo oxide film annealed in pure hydrogen. In particular, the band of the doubly coordinated oxygens shows considerably smaller shift to lower wavenumbers (871 → 788 cm^{-1}; $\Delta\nu$ = -83 cm^{-1}), whereas the band of the terminal oxygens only decreases in intensity, without presenting a significant shift. In addition, the band at *ca.* 350 cm^{-1} does not appear in this

case. Moreover, a new band at *ca.* 1170 cm^{-1} attributed possibly to the deformation mode of Mo−O−H bonds (δMo−O−H) appears.[11] The structural changes of the molybdenum oxide films studied with Raman spectroscopy, were also studied with FT-IR spectroscopy (Figure S5 b). In brief, from the analysis of the FT-IR spectra, the following observations were made that are in accordance with the results obtained by Raman spectroscopy: (a) Upon increasing the amount of hydrogen in the annealing environment a shift of the νO−Mo_2 band to lower wavenumbers (868 → 721 → 683 cm^{-1}) is detected, confirming therefore the under-stoichiometry of the films (b) Similarly, the band of the νO═Mo shifts to higher wavenumbers (948 → 973 → 975 cm^{-1}). In the case of pure H_2 annealed film a new band appears at 1107 cm^{-1} attributed to the bending mode of Mo−OH bonds (δMo−OH); a result that has been reported in literature for both molybdenum bronzes (H_xMoO_3) and tungsten bronzes (H_xWO_3).[12]

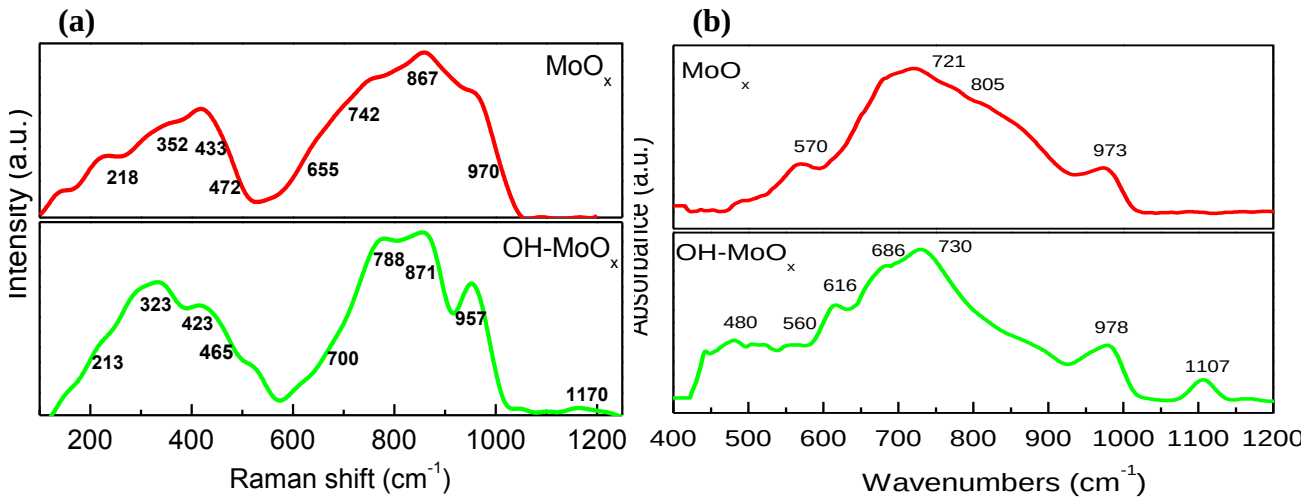

Figure S5. (a) Raman and (b) FTIR spectra taken on molybdenum oxide samples deposited under reducing ambient and then annealed in environment containing low (MoO_x) and high hydrogen content (OH-MoO_x).

S2.3 Photoluminescence spectra and conductivity measurements

In Figure S6 PL spectra for molybdenum oxide films annealed in FG and H_2 environments, are shown. It can be observed that both films exhibit similar broad emission spectra (with the one annealed in H_2 to exhibit a more intense signal) which also present significant similarities with the PL spectrum of OH-WO_x, shown above. The broad emission can be attributed to the midgap states, present in the UPS spectra of both oxides.

To examine electron transport in the two Mo oxide films we investigated the temperature dependence of their electrical resistivity in 10 nm thick films and the results are shown in Figure S6 b. A gradual decrease of the resistivity with temperature can be clearly seen. Again, film annealed in H2 exhibits slightly reduced resistivity compared with the one annealed in FG.

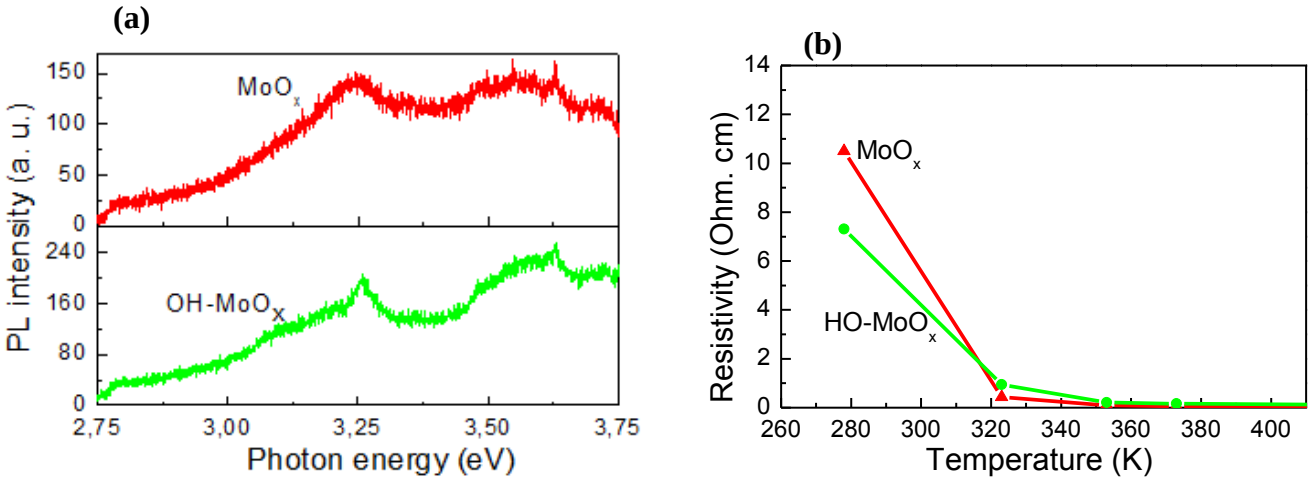

Figure S6. (a) Photoluminescence spectra taken on molybdenum oxides deposited in environment containing low (MoO_x) and high hydrogen content (OH-MoO_x) with excitation radiation of 3.81 eV. (b) Resistivity measurements vs temperature for both tungsten oxide, 10 nm thin films.

S3. Comparative study on ZnO and OH-ZnO films: Structure ans Electric Transport

S3.1 X-ray (XPS) and ultraviolet (UPS) photoelectron spectra

The XPS data for ZnO films annealed at different environments (Figure S7) show that the Zn $2p_{3/2}$ and the Zn $2p_{1/2}$ lines are found at the binding energies of about 1021 eV and 1045 eV in both cases, indicating that both films are stoichiometric (ZnO). In the XPS O 1s data the situation is different; film annealed in FG exhibits lower amount of surface hydroxyl groups, mainly in the form of water molecules, while that annealed in H_2 show a high amount of surface hydroxyl groups bonded to metal cations. Finally, UPS spectra of both films show significant similarities regarding the estimating W_F values (about 4.4 eV) and the valence band onset (about 3.0 eV) (Figure S7 e), however, the UPS spectrum of the film annealed in H_2 exhibits a clear tail in the near Fermi level region, an indication for the formation of midgap states which are

not present in the spectrum of the film annealed in FG. The optical bandgap was estimated about 3.3 eV in both films.

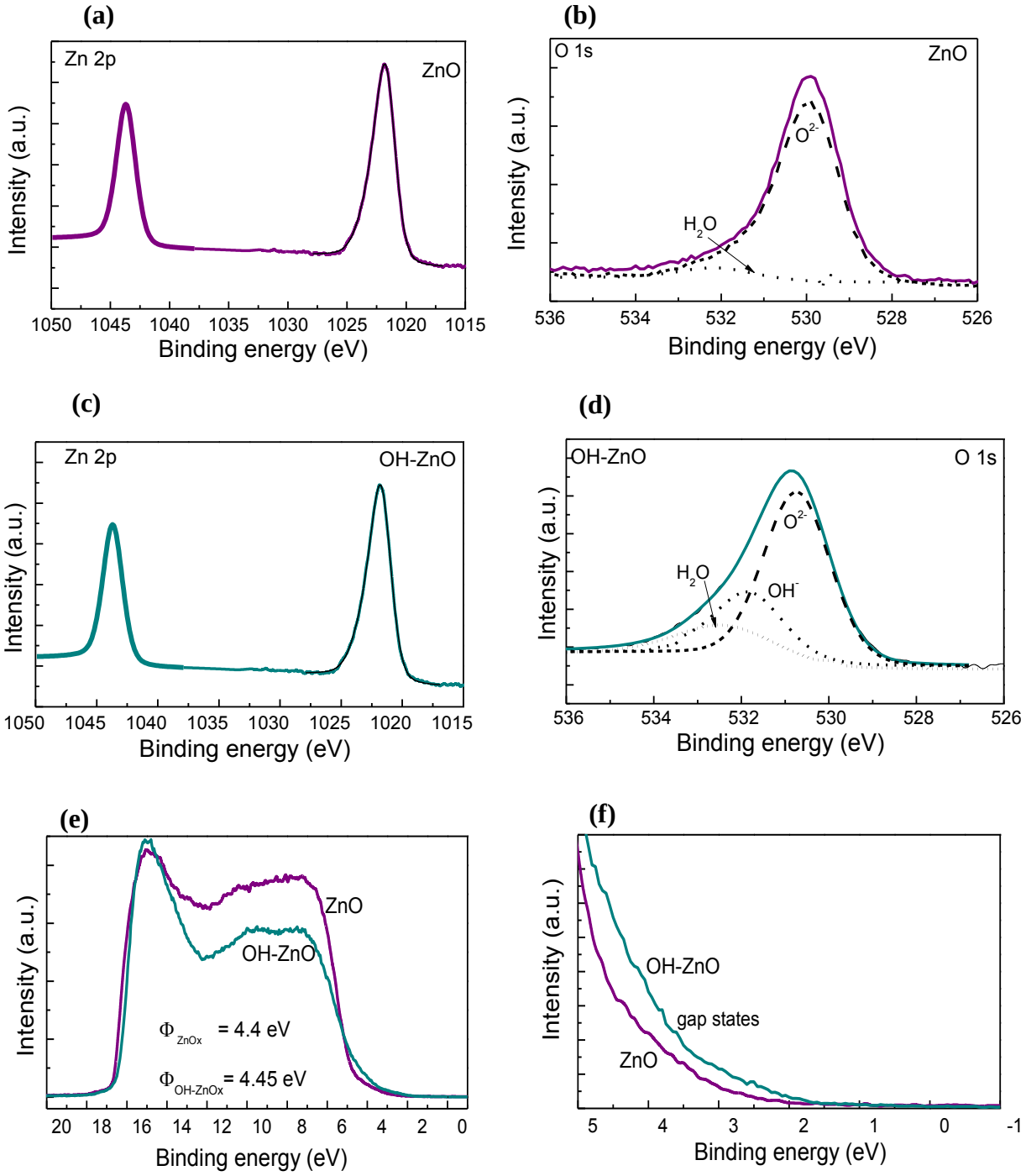

Figure S7 XPS (and fittings) and UPS spectra of zinc oxides annealed in environment containing low (ZnO) and high hydrogen content (OH-ZnO). (a) and (c) Zn 2p XPS core levels and (b) and (d) O 1s core leves of ZnO and OH-ZnO, respectively. (e) The valence band spectra derived from UPS measurements taken on ZnO and OH-ZnO films. (f) The near Fermi level region of the UPS spectra.

S3.2 Raman and FTIR measurements

The room temperature Raman spectra of ZnO samples annealed in different environments were nearly identical. The Raman band modes identified were the E_2 (high) at 435 cm^{-1}, A_1 longitudinal optical (LO) at 543 cm^{-1}, E_1 longitudinal optical (LO) at 566 cm^{-1} and a secondary A_1 longitudinal optical (2LO) at 1105 cm^{-1}.[13] For the sample annealed in H_2, however, the intensity of the Raman peaks were slightly shifted (e. g., the peak at 483 cm^{-1}, Figure S8 a) which may be an indication of surface hydrogenation of the sample. The room temperature FTIR spectra of both ZnO films also showed significant similarities (Figure S8 b).The main difference in these spectra is related to the vibrations of H-O-H and Zn-OH and appear in the region of 3000-3600 cm^{-1} where vibrations due to the presence of Zn-OH and of adsorbed H_2O appear. The spectrum of the sample annealed in H_2 exhibits clear peaks in the aforementioned area, while such peaks are absent from the spectrum of the film annealed in FG.

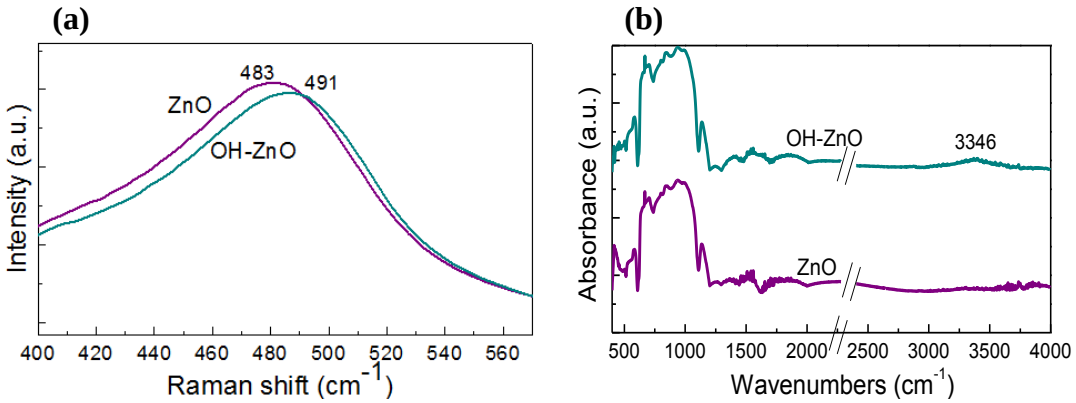

Figure S8. (a) FTIR spectra taken on zinc oxides annealed in environment containing low (ZnO) and high hydrogen content (OH-ZnO). (b) Photoluminescence spectra taken on of zinc oxides deposited in environment containing low (ZnO) and high hydrogen content (OH-ZnO) with excitation radiation of 3.81 eV. (c) Resistivity measurements vs temperature for both tungsten oxide, 10 nm thin films.

S3.3 Photoluminescence spectra and conductivity measurements

Figure S9 a shows the PL spectra obtained at room temperature for the two ZnO thin films. PL spectra in both samples exhibit two emission peaks which show the UV emission peaks at near band edge and a broad green-yellow radiation at ~470–660 nm region which can be attributed to surface/bulk defects/traps. For the

film annealed in H_2 the trap assisted emission is significantly quenched, emission is quenched. This indicates that the incorporation of hydrogen into ZnO surface/bulk suppresses the trap emission.

The resistivity plot (Figure S9 b) of both films exhibit nearly the same dependence versus temperature with slightly increased conductivity for the one annealed in H_2 environment.

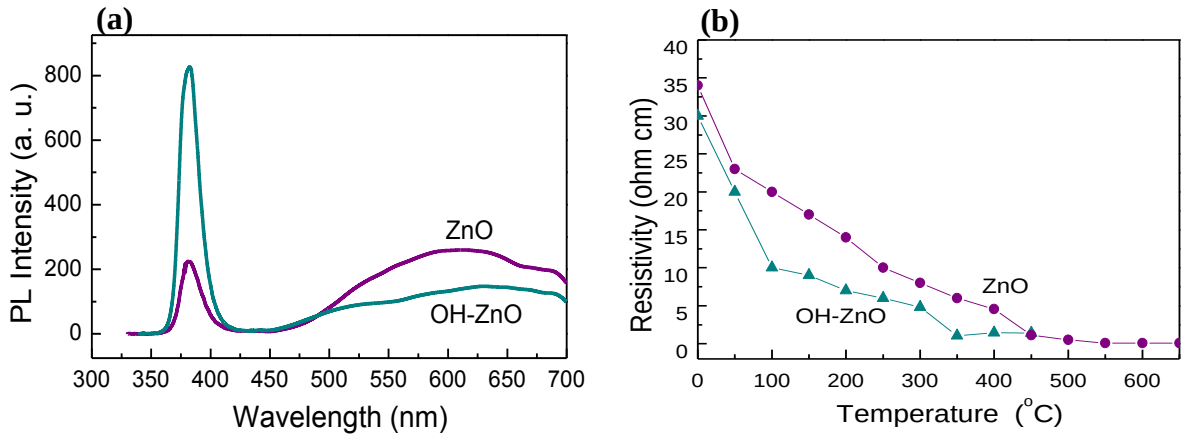

Figure S9. (a) Photoluminescence spectra taken on of zinc oxides deposited in environment containing low (ZnO) and high hydrogen content (OH-ZnO) with excitation radiation of 3.81 eV. (b) Resistivity measurements vs temperature for both tungsten oxide, 10 nm thin films.

S4. Comparative study on TiO_2 and OH-TiO_2 films: Structure ans Electric Transport

S4.1 X-ray (XPS) and ultraviolet (UPS) photoelectron spectra

The XPS data for TiO_2 samples annealed in FG and H_2 environment revealed no differences between these samples (Figure S10 a and c). The Ti $2p_{3/2}$ and Ti $2p_{1/2}$ peaks positions at 458.4 eV and 464.4 eV are characteristic of Ti^{4+} in TiO_2.[14] The XPS O 1s spectrum of the film annealed in FG could be deconvoluted into two component peaks (Figure S10 b), wherein the lowest energy peak (529.7 eV) was assigned to lattice oxygen (O^{2-}) in TiO_2 and the highest energy peak to oxygen in absorbed water molecules (532.6 eV). In the spectrum of the sample annealed in H_2 an additional broad middle peak (531.5 eV) corresponding to Ti−OH surface hydroxyl species has a significant contribution. The total Ti:O ratio did not vary significantly between the samples, although the -OH:O^{2-} ratio increased, indicating that the surface stoichiometry of the

TiO_2 remained relatively unchanged, apart from the increase in the concentration of surface hydroxyl groups in the H_2 annealed sample. The UPS spectra of these films remained virtually identical in the secondury electron region (estimated work function about 4.0 eV, Figure S10 e) indicating nearly the same value of W_F for both films, whereas a significant shift of the valence band edge (located at about 2.9 eV) towards the Fermi level due to introduction of midgap states in the H_2 annealed film, was observed (Figure S10 f).

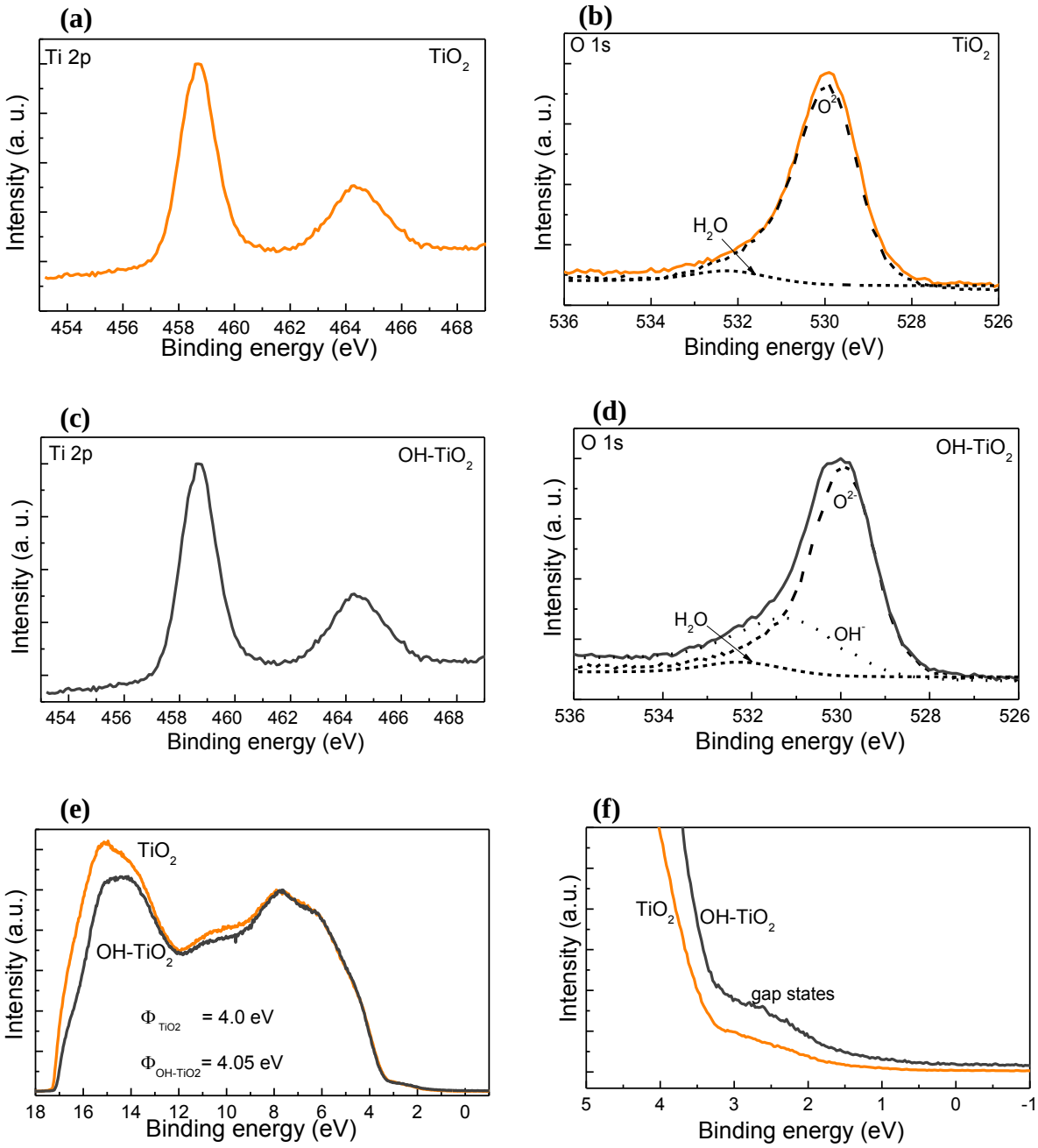

Figure S10 XPS (and fittings) and UPS spectra of titanium oxides annealed in environment containing low (TiO_2) and high hydrogen content (OH-TiO_2). (a) and (c) Ti 2p XPS core levels and (b) and (d) O 1s core leves of TiO_2 and OH-TiO_2, respectively. (e) The valence band spectra derived from UPS measurements taken on TiO_2 and OH-TiO_2films. (f) The near Fermi level region of the UPS spectra.

S4.2 Raman and FTIR measurements

Raman spectroscopy revealed significant similarities between the spectra of these samples with the main difference to be the small peak broadening and shifting for the sample annealed in H_2 (e. g., th peak shown in Figure S11 a). The peak broadening effect and shift has been observed in several recent studies on hydrogenated TiO_2, and is attributed to the presence of lattice disordered.[14]

From the following FT-IR spectra of these samples (Figure 11 b) it can be seen that by increasing the hydrogen content in the annealing environment the large broad peak at the 3000-3600 cm^{-1} increases significantly in intensity. This peak can be assigned to water or hydroxyl species in general bound in the materials surface or/and bulk.

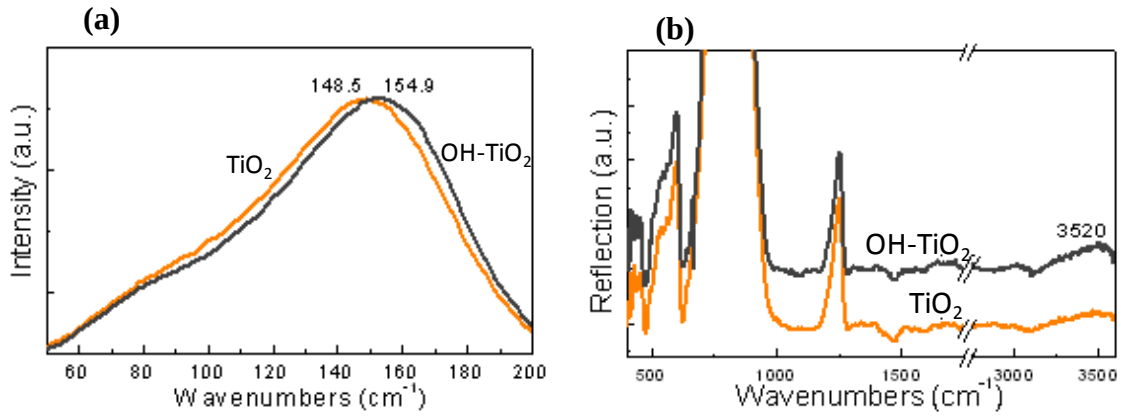

Figure S11. (a) Raman and (b) FTIR spectra taken on titanium oxides deposited in environment containing low (TiO_2) and high hydrogen content (OH-TiO_2).

S4.3 Photoluminescence spectra and conductivity

The PL spectra of TiO_2 samples in the wavelength range of 350-650 nm with the excitation at 320 nm are shown in Figure S12 a. Their emission spectra shapes are very similar. Three main emission peaks are located at about 380 nm (3.3 eV), 415 nm (3.0 eV), 440 nm (2.8 eV) and 465 nm (2.7 eV), respectively. The first one is attributed to the emission of bandgap transition corresponding to the bandgap energy of anatase TiO2 (about 3.3 eV). The peak at 415 nm is attributed to band edge free excitons. The other two peaks at 440 nm and 465 nm may mainly result from surface defects of the TiO_2 samples. The PL peak intensity of

the OH-TiO_2 sample (annealed in H_2) reveals a significant decrease compared with TiO_2 (annealed in FG). This result indicates that the latter samples have a relative low recombination rate of electrons and holes. Normally, low recombination rate of electrons and holes are expected from samples with passivated surface (and/or bulk) traps/defects which, in our case, may be attributed to passivation of surface dangling bonds with hydroxyl groups. The resistivity vs temperature plot (Figure S12 b) shows that, as in the cases of other metal oxides shown above, the sample annealed in hydrogen environment exhibits slightly increased conductivity relative to the sample annealed in FG for temperatures ranging from room temperature up to 250 ^oC.

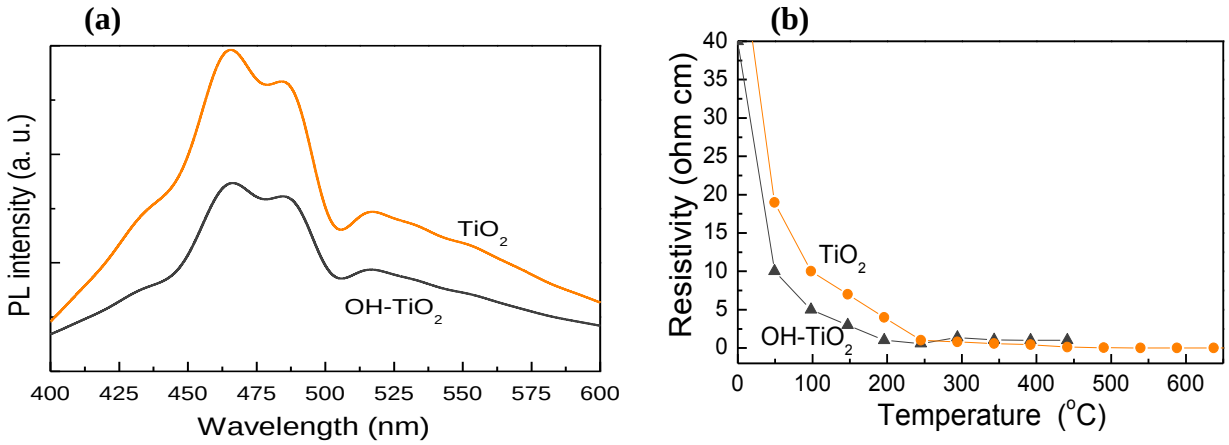

Figure S12. (a) Photoluminescence spectra taken on of zinc oxides deposited in environment containing low (TiO_2) and high hydrogen content (OH-TiO_2) with excitation radiation of 3.81 eV. (b) Resistivity measurements vs temperature for both tungsten oxide, 10 nm thin films.

S5. Steady state PL spectra of polymer blend films

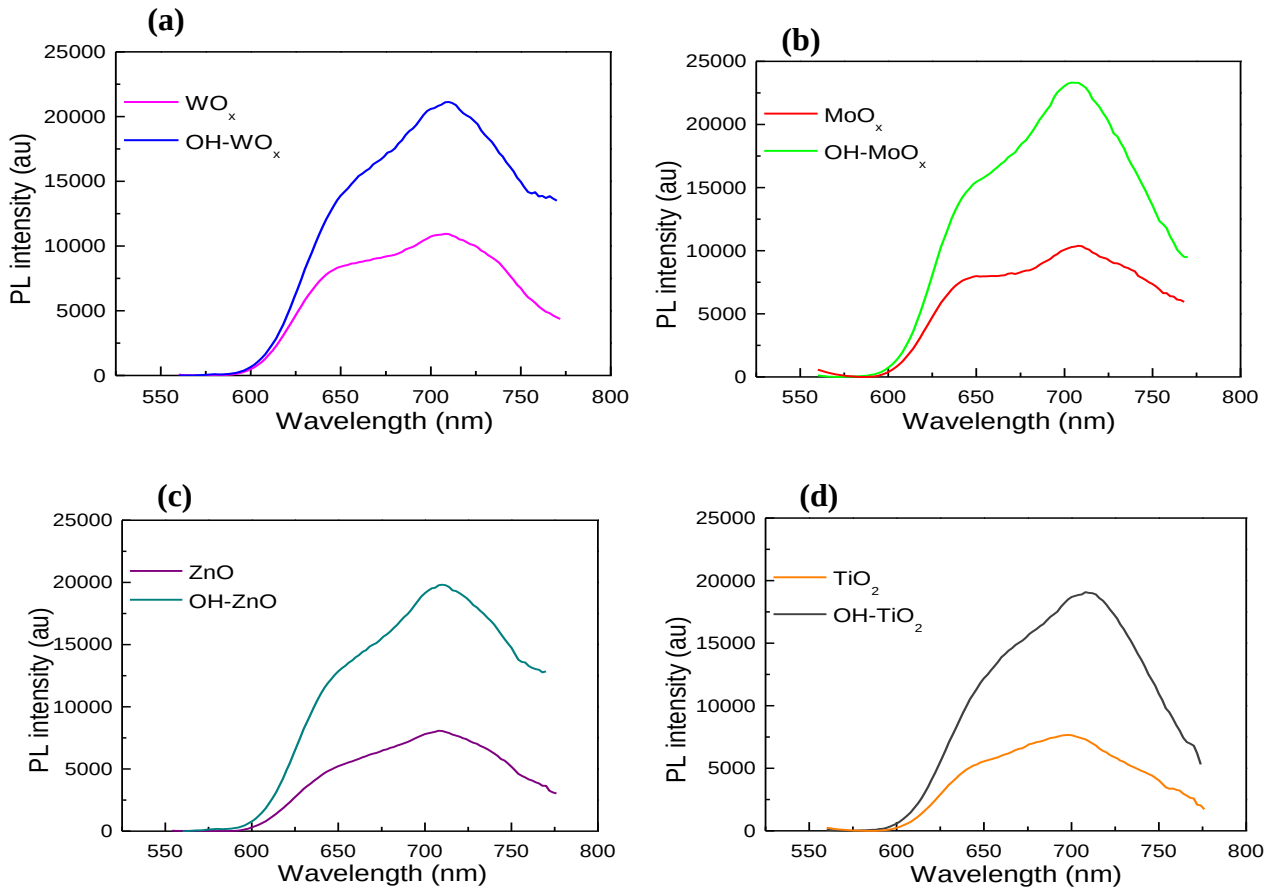

Figure S13 Steady-state photoluminescence spectra of P3HT:$PC_{71}BM$ photoactive layer spin coated on top of the different metal oxide substrates. The thickness of the active layer was 150 nm and it was thermally annealed at 70 ^{o}C for 5 min.

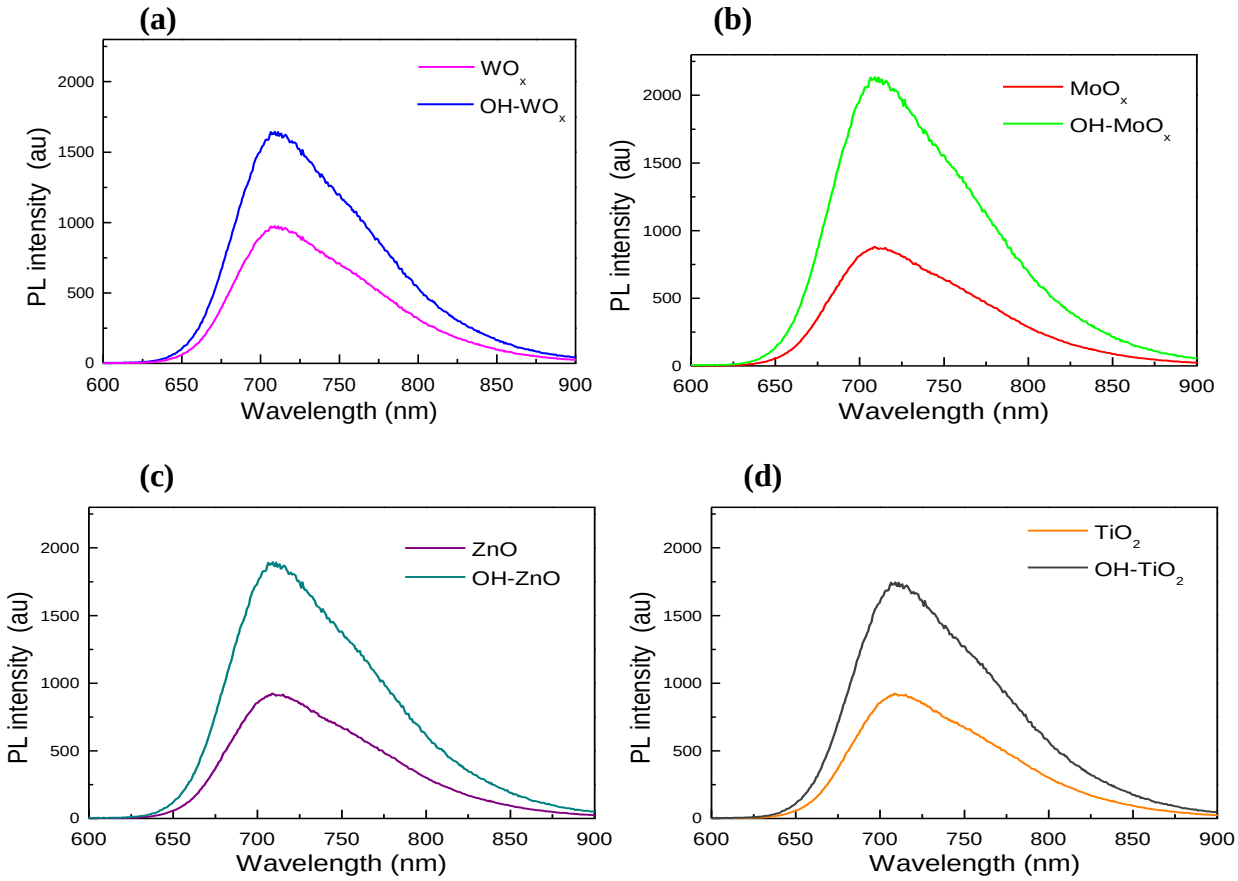

Figure S14 Steady-state photoluminescence spectra of PCDTBT:$PC_{71}BM$ photoactive layer spin coated on top of the different metal oxide substrates. The thickness of the active layer was 150 nm and it was thermally annealed at 70 ^{o}C for 5 min.

S6. Tables

Table S1: Synopsis of composition and electronic properties of the metal oxide surfaces of this study.

Metal oxide bottom electrode	XPS M core levels			XPS O 1s peak	Oxide work function (eV)
	M^{n+} (*)	$M^{(n-1)+}$		H_2O+OH^-/O_2^-	
WO_x	75% (n=6)	25 (n=5)		8%	5.80
OH-WO_x	73% (n=6)	27% (n=5)		32%	5.80
MoO_x	78% (n=6)	22% (n=5)		10%	5.90
H-MoO_x	76% (n=6)	24% (n=5)		45%	5.90
ZnO	100% (n=2)	0%		5%	4.40
OH-ZnO	100% (n=2)	0%		38%	4.45
TiO_2	100% (n=4)	0%		3%	4.00
OH-TiO_2	100% (n=4)	0%		35%	4.05

(*) n: the highest oxidation state of the corresponding metal cation

Table S2. Device characteristics of P3HT:PC_{71}BM-based cells with the conventional architecture ITO/WO_x, MoO_x, OH-WO_x, OH-MoO_x 20 nm/ P3HT:PC_{71}BM 150 nm/PW-12 POM 5 nm/Al or the reverse architecture FTO/ ZnO, OH-ZnO, TiO_2, OH-TiO_2 30 nm/ P3HT:PC_{71}BM 150 nm/OH-MoO_x 10 nm/Al.

Metal oxide substrate	Jsc (mA/cm^2)	Voc (V)	FF	PCE (%)
WO_x	**9.35** 9.25(±0.10)	**0.62** 0.60(±0.02)	**0.56** 0.54(±0.02)	**3.2** 3.1(±0.1)
OH-WO_x	**10.25** 10.20 (±0.10)	**0.68** 0.67(±0.01)	**0.60** 0.58(±0.02)	**4.2** 4.1(±0.1)
MoO_x	**9.45** 9.35(±0.10)	**0.62** 0.60(±0.02)	**0.58** 0.56(±0.02)	**3.4** 3.3(±0.1)
OH-MoO_x	**10.45** 10.35 (±0.10)	**0.69** 0.68(±0.01)	**0.62** 0.60(±0.02)	**4.5** 4.4(±0.1)
ZnO	**9.25** 9.15(±0.10)	**0.63** 0.61(±0.02)	**0.58** 0.56(±0.02)	**3.4** 3.3(±0.1)
OH-ZnO	**10.35** 10.25 (±0.10)	**0.69** 0.68(±0.01)	**0.61** 0.59(±0.02)	**4.4** 4.3(±0.1)
TiO_2	**9.20** 9.10(±0.10)	**0.63** 0.62(±0.02)	**0.58** 0.56(±0.02)	**3.4** 3.2(±0.1)
OH-TiO_2	**10.30** 10.20 (±0.10)	**0.68** 0.66(±0.02)	**0.60** 0.58(±0.02)	**4.2** 4.1(±0.1)

Data and statistics based on 32 cells of each type. Numbers in bold are the maximum recorded values.

Table S3. Device characteristics of PCDTBT:$PC_{71}BM$-based OPV cells with the conventional architecture ITO/WO_x, MoO_x, OH-WO_x, OH-MoO_x 20 nm/ PCDTBT:$PC_{71}BM$ 100 nm/PW-12 POM 5 nm/Al or the reverse architecture FTO/ ZnO, OH-ZnO, TiO_2, OH-TiO_2 30 nm/ P3HT:$PC_{71}BM$ 150 nm/OH-MoO_x 10 nm/Al.

Metal oxide layer	Jsc (mA/cm^2)	Voc (V)	FF	PCE (%)
WO_x	**9.90** 9.80 (±0.10)	**0.82** 0.81(±0.01)	**0.69** 0.67(±0.02)	**5.6** 5.7(±0.1)
OH-WO_x	**10.90** 10.80 (±0.10)	**0.88** 0.87(±0.01)	**0.73** 0.71(±0.02)	**7.0** 6.9(±0.1)
MoO_x	**9.95** 9.85 (±0.10)	**0.82** 0.81(±0.01)	**0.70** 0.68(±0.02)	**5.7** 5.6(±0.1)
OH-MoO_x	**11.05** 10.95 (±0.10)	**0.89** 0.88(±0.01)	**0.73** 0.71(±0.02)	**7.2** 7.1(±0.1)
ZnO	**9.70** 9.60 (±0.10)	**0.83** 0.82(±0.01)	**0.69** 0.67(±0.02)	**5.6** 5.7(±0.1)
OH-ZnO	**11.00** 10.90 (±0.10)	**0.89** 0.88(±0.01)	**0.73** 0.71(±0.02)	**7.1** 7.0(±0.1)
TiO_2	**9.60** 9.50 (±0.10)	**0.83** 0.82(±0.01)	**0.69** 0.67(±0.02)	**5.5** 5.4(±0.1)
OH-TiO_2	**10.80** 10.80 (±0.10)	**0.88** 0.87(±0.01)	**0.73** 0.71(±0.02)	**7.0** 6.9(±0.1)

Data and statistics based on 32 cells of each type. Numbers in bold are the maximum recorded values.

S7 References

1. D. Barreca, G. Carta, A. Gasparotto, G. Rossetto, E. Tondello, P. Zanella, *Surf. Sci. Spectra*, 2001, **8**, 258.
2. G. Dickens, S. Crouch-Baker, M. Weller, *Sol. Sate Ionics*, 1986, **18/19**, 89.
3. H. Höchst, R. D. Bringans, *Appl. Surf. Sci.*, 1982, **11/12**, 768.
4. C. Wagner, L. Davis, M. Zeller, L. Taylor, R. Raymond, L. Gale, *Surf. Interf. Anal.*, 1981, **3,** 211.
5. F. Daniel, B. Desbat, J. C. Lassegues, B. Gerand, M. Figlarz, *J. Solid State Chem.*, 1987, **67**, 235.
6. M. Yalamanchili A. Atia, J. Miller, *Langmuir*, 1996**, 12** 4176.
7. K. Lee, W S. Seo, J. T. Park, *J. Am. Chem. Soc.*, 2003, **125**, 3408.
8. M. T. Greiner, M.G. Helander, W.-M. Tang, Z.-B. Wang, J. Qiu, Z.-H. Lu, *Nature Materials*, 2012, **11**, 76.
9. K. Ajito, L. A. Nagahara, D. A. Tryk, K. Hashimoto, A. Fujishima, *J. Phys. Chem.* 1995, **99**, 16383.
10. Vasilopoulou, M.; Douvas, A.M.; Georgiadou, D.G.; Palilis, L.C.; Kennou, St.; Sygellou, L.; Soultati, A.; Kostis, I.; Papadimitropoulos, G.; Davazoglou, D.; Argitis, P. *J. Am. Chem. Soc.* **2012**, *134*, 16178-16187.
11. Seguin, L.; Figlarz, M.; Cavagnat, R.; Lassègues, J.-C. *Spectrochimica Acta A* **1995**, *51*, 1323-1344.
12. P. Yang, X. Xiao, Y. Li, Y. Ding, P. Quiang, X. Tan, W. Mai, Z. Lin, W. Wu, T. Li, H. Jin, P. Liu, J. Zhou, C. P. Wong, Z. L. Wang, *ACS Nano*, 2013, **7**(3), 2617.
13. K. W. J Wong, M. R. Field, J. Z. Ou, K. Latham, M. J. S Spencer, I. Yarovsky, K. Kalantar-zadeh, *Nanotechnology*, 2012, **23**, 015705.
14. T. Leshuk, R. Parviz, P. Everett, H. Krishnakumar, R. A. Varin, R. F. Gu, *ACS Appl. Mater. Interfaces* 2013, **5**, 1892.